Derivation of the nonholonomic equations of motion for an unmanned ground vehicle mounted with a launching device

Tran Xuan Dieu*

Institute of Missile, Academy of Military Science and Technology, 17 Hoang Sam, Nghia Do, Hanoi, Vietnam.

*Corresponding author: xuandieuvtl@gmail.com

Received 15 Jun. 2026; Revised 20 Aug. 2026; Accepted 04 Sep. 2026; Published 16 Sep. 2026.

DOI: https://doi.org/10.54939/1859-1043.j.mst.FMC.2026.80-89

ABSTRACT

In this paper, a non-holonomic dynamic model of an unmanned ground vehicle (UGV) mounted with a launcher (LV) is established based on the Lagrange equations with multipliers. The inverse dynamic model of the UGV-LV mechanical system is formulated as a basis to determine the required wheel-axle torque laws for tracking target trajectories, as well as the dynamic nature of the Lagrange multipliers. The integrated UGV-LV dynamic model serves as the basis for the structural design of the UGV-LV and the synthesis of its controller.

Keywords: Unmanned ground vehicle; Nonholonomic system; Lagrange multiplier; Pseudoinverse matrix.

1. INTRODUCTION

UGVs typically navigate complex terrains while carrying an LV that demands high-precision elevation and azimuth control. From a mechanical standpoint, the UGV platform, due to its wheeled locomotion, constitutes a nonholonomic system, when integrated with an LV, the combined UGLV inherits this nonholonomic property. Dynamic modeling of UGVs remains a highly relevant research domain that has attracted a vast body of literature. Unlike holonomic systems, which are governed exclusively by geometric constraints, nonholonomic systems are subjected to additional kinematic constraints. These are characterized by non-integrable, first-order differential equations that couple the system's velocity components, thereby rendering the formulation of nonholonomic equations of motion far more complex than that of holonomic counterparts.

Among the published literature, Albagul and Wahyudi [1] presented significant results on the dynamics and control of a mobile module. In their dynamic model, the authors formulated the nonholonomic constraint equations for a UGV undergoing planar motion. The system of non-holonomic constraint equations developed by the authors for the case of a UGV moving on a plane, combined with the equations of motion, was used to synthesize the controller. Additionally, Chu Anh My et al.[2] published findings on establishing the dynamic equations for a UGV propelled by omnidirectional (Omni) wheels. Anna Jaskot and Bogdan Posiadala [3] developed a dynamic model for UGVs under unstable conditions with non-collinear wheel steering orientations. Igor Zeidis and Klaus Zimmermann [4] formulated the dynamics of a UGV equipped with Mecanum wheels, a configuration widely adopted for indoor mobile robots. Furthermore, Jiri Balla [5], J.Dziopa [6] investigated the vibration responses of a UGLV system subjected to firing forces. In general, existing literature has predominantly focused either on the independent dynamics of the UGV platform or on the vibration analysis of the vehicle during stationary firing. The coupled dynamic behavior of the integrated UGLV system during on-the-move operations remains unaddressed. Moreover, the conventional governing equations of motion have been limited to the operational space formulation. In practice, these equations are highly challenging to implement in control law synthesis due to the significant errors and difficulties associated with feedback signals regarding the UGV's center of mass and orientation. To overcome this limitation, this paper presents the formulation of the dynamic equations for the coupled UGLV platform undergoing

simultaneous motion. Utilizing a multibody dynamics approach, the kinematic relations, nonholonomic constraints, and equations of motion are systematically derived in a concise and explicit closed-form. Furthermore, Lagrange multipliers are eliminated to reduce the governing differential equations of motion into a minimal form within the joint space. Combined with the nonholonomic constraints, these reduced formulations yield a system of differential-algebraic equations ideally suited for both structural design and control loop synthesis. The validity of all intermediate analytical steps in this derivation has been cross-verified using Maple and MATLAB. The remainder of this paper is organized as follows: development of the mathematical model, result simulation based on a set of initial parameters, discussion, and conclusion.

2. MATHEMATICAL MODEL

2.1. Kinematics model

The mechanical system, illustrated in Figure 1, comprises two main interconnected rigid bodies: (1) a UGV platform configured with two rear driving wheels and a front castor wheel, whose dimensions and mass are negligible compared to those of the UGV and LV, and are thus omitted from the mechanical formulation; and (2) a launching vehicle (LV) attached to the UGV body via a revolute joint aligned with the vehicle's center of mass, without loss of generality. Driven by independent torques applied to the left and right wheels, the UGV is capable of maneuvering across any location on an infinitely rigid ground plane.

The mathematical model of the mechanical system is formulated based on the following assumptions: (i) all components within the system, including the vehicle chassis, left and right wheels, and the LV, are treated as perfectly rigid bodies; (ii) the UGV navigates exclusively on a flat and infinitely rigid surface; (iii) the driving wheels satisfy pure rolling conditions without slipping; (iv) all kinematic joints are assumed to be frictionless; and (v) the mass and inertia of the castor wheel are negligible relative to the entire system.

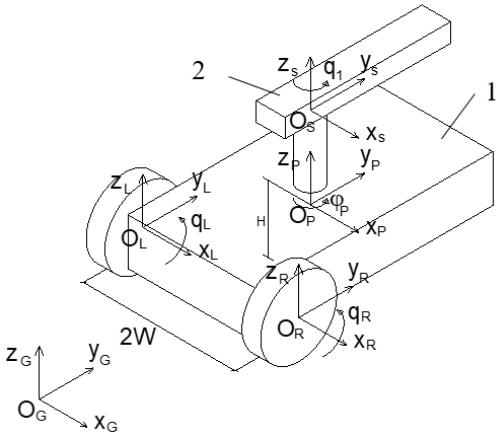


Figure 1. *Kinematic model of the UGLV.*

To formulate the mathematical model, the following reference frames are established:

$O_G(x_G, y_G, z_G)$: The global inertial reference frame fixed to the ground plane; $O_P(x_P, y_P, z_P)$: The body-fixed coordinate system attached to the vehicle chassis; $O_L(x_L, y_L, z_L)$: The wheel-fixed coordinate system attached to the left driving wheel; $O_R(x_R, y_R, z_R)$: The wheel-fixed coordinate system attached to the right driving wheel; $O_S(x_S, y_S, z_S)$: The coordinate system fixed to LV.

$q_w = [q_L \quad q_R]^T \in \mathbb{R}^2$: The vector representing the angular displacements (rotation angles) of the left and right driving wheels; $q_p = [x_p \quad y_p \quad \varphi_p]^T \in \mathbb{R}^3$ The vector of generalized coordinates of the vehicle chassis; q_1 – The generalized coordinate of the LV;

The total vector of generalized coordinates investigated within the system configuration is defined as: $\mathbf{q}_e = [q_L \quad q_R \quad x_P \quad y_P \quad \varphi_P \quad q_1]^T \in R^6$

2.1.1. Forward kinematics

- The direction cosine matrix (rotation matrix) mapping the wheel frame O_L to the chassis frame O_P is expressed as:

$$\mathbf{A}_{\mathrm{PL}} = \begin{bmatrix} 1 & 0 & 0 \\ 0 & \cos(q_L) & -\sin(q_L) \\ 0 & \sin(q_L) & \cos(q_L) \end{bmatrix} \tag{1}$$

- The direction cosine matrix mapping the frame O_R to the frame O_P is expressed as:

$$\mathbf{A}_{\mathrm{PR}} = \begin{bmatrix} 1 & 0 & 0 \\ 0 & \cos(q_R) & -\sin(q_R) \\ 0 & \sin(q_R) & \cos(q_R) \end{bmatrix} \tag{2}$$

- The direction cosine matrix mapping the frame O_P to the frame O_G is expressed as:

$$\mathbf{A}_{\mathrm{GP}} = \begin{bmatrix} \cos(\varphi_P) & -\sin(\varphi_P) & 0 \\ \sin(\varphi_P) & \cos(\varphi_P) & 0 \\ 0 & 0 & 1 \end{bmatrix} \tag{3}$$

- The direction cosine matrix mapping the frame O_S to the frame O_P is expressed as:

$$\mathbf{A}_{\mathrm{PS}} = \begin{bmatrix} \cos(q_1) & -\sin(q_1) & 0 \\ \sin(q_1) & \cos(q_1) & 0 \\ 0 & 0 & 1 \end{bmatrix} \tag{4}$$

- The direction cosine matrix mapping the frame O_R to the frame O_G is expressed as:

$$\mathbf{A}_{\mathrm{R}} = \mathbf{A}_{\mathrm{GP}}\mathbf{A}_{\mathrm{PR}}\ ;\ \mathbf{A}_{\mathrm{L}} = \mathbf{A}_{\mathrm{GP}}\mathbf{A}_{\mathrm{PL}}\ ;\ \mathbf{A}_{\mathrm{S}} = \mathbf{A}_{\mathrm{GP}}\mathbf{A}_{\mathrm{PS}} \tag{5}$$

- The position vector of the origin O_P expressed in the frame O_G is expressed as:

$$\mathbf{r}_{OP} = \begin{bmatrix} x_P & y_P & R+H \end{bmatrix}^T \tag{6}$$

The position vector of the origin O_L expressed in the frame O_G:

$$\mathbf{r}_{OL} = \mathbf{r}_{OP} + \mathbf{A}_{GP}\mathbf{r}_{OLP} = \begin{bmatrix} x_P - W\cos(\varphi_P) + e\sin(\varphi_P) \\ y_P - W\sin(\varphi_P) - e\cos(\varphi_P) \\ R \end{bmatrix} \tag{7}$$

The position vector of the origin O_R expressed in the frame O_G as:

$$\mathbf{r}_{OR} = \mathbf{r}_{OP} + \mathbf{A}_{GP}\mathbf{r}_{ORP} = \begin{bmatrix} x_P + W\cos(\varphi_P) + e\sin(\varphi_P) \\ y_P + W\sin(\varphi_P) - e\cos(\varphi_P) \\ R \end{bmatrix} \tag{8}$$

The position vector of the origin O_S expressed in the frame O_G as:

$$\mathbf{r}_{OS} = \mathbf{r}_{OP} + \mathbf{A}_{GP}\mathbf{r}_{OSP} = \begin{bmatrix} x_P & y_P & R+H+h \end{bmatrix}^T \tag{9}$$

The position vector of the LV center of mass O_S expressed in the frame O_G as:

$$\mathbf{r}_{CS} = \mathbf{r}_{OS} + \mathbf{A}_S\mathbf{r}_{CSS} = \begin{bmatrix} x_P - r\cos(\varphi_P)\sin(q_1) - r\sin(\varphi_P)\cos(q_1) \\ y_P + r\cos(\varphi_P)\cos(q_1) - r\sin(\varphi_P)\sin(q_1) \\ R+H+h \end{bmatrix} \tag{10}$$

Consequently, the formulations from (1) to (10) fully parameterize the geometric configuration of UGLV model. The mathematical expressions for identifying the system's kinematic parameters are detailed below.

The determination of the angular velocity for each rigid body within the frame O_G is based on the skew-symmetric matrix (hat operator) of the angular velocity vector. This skew-symmetric operator is defined by the following formulation [7]:

$$\tilde{\boldsymbol{\omega}} = \dot{\mathbf{A}}\mathbf{A}^T \tag{11}$$

From this kinematic operator, the components of the angular velocity vector for individual bodies can be readily obtained.

The angular velocity vector of the left wheel, the right wheel, vehicle chassis and LV resolved in the frame O_G is

$$\boldsymbol{\omega}_L = \begin{bmatrix} \dot{q}_L \cos(\varphi_P) \\ \dot{q}_L \sin(\varphi_P) \\ \dot{\varphi}_P \end{bmatrix};\ \boldsymbol{\omega}_R = \begin{bmatrix} \dot{q}_R \cos(\varphi_P) \\ \dot{q}_R \sin(\varphi_P) \\ \dot{\varphi}_P \end{bmatrix};\boldsymbol{\omega}_P = \begin{bmatrix} 0 \\ 0 \\ \dot{\varphi}_P \end{bmatrix};\ \boldsymbol{\omega}_S = \begin{bmatrix} 0 \\ 0 \\ \dot{q}_1 + \dot{\varphi}_P \end{bmatrix} \tag{12}$$

The linear velocity of the center of mass is determined through the derivative of the center of mass's coordinate with respect to time.

A critical aspect investigated in this system is the nonholonomic constraint formulation. It is readily apparent that employing all six generalized coordinates within the vector introduces redundancy, given that a subset of only three independent generalized coordinates such as q_L, q_R and q_1 is sufficient to fully parameterize the configuration space of LV. Consequently, these six coordinates are interdependent; selecting any three coordinates allows the remaining ones to be implicitly coupled through constraint equations. Although variations in the generalized coordinates q_L, q_R and q_1 alter the spatial pose of LV, unlike conventional serial or parallel manipulators, no direct algebraic geometric constraints can be established among these variables to uniquely define the robot's position. Instead, the spatial positioning of LV is governed by wheel-ground physical interactions, which are mathematically manifested as non-integrable kinematic constraints in velocity form.

Based on the idealized pure rolling without slipping assumption, the absolute linear velocity at the center of mass of LV is derived directly from the wheel kinematic states specifically, the angular velocities of the two independent driving wheels, $\dot{q}_L$ and $\dot{q}_R$.

At any given instant, there always exists an instantaneous center of rotation, denoted as M, for the chassis. From the velocity distribution depicted in Figure 2, the following relationship can be readily derived:

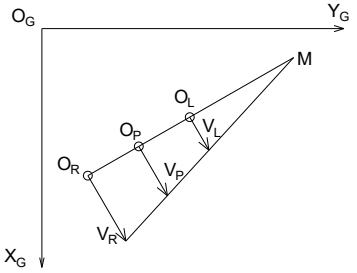


Figure 2. *Schematic for determining the velocity at the chassis center of mass.*

$$\begin{bmatrix} \dot{x}_P \\ \dot{y}_P \\ \dot{\varphi}_P \end{bmatrix} = \begin{bmatrix} \frac{R\sin(\varphi_P)}{2} & \frac{R\sin(\varphi_P)}{2} \\ -\frac{R\cos(\varphi_P)}{2} & -\frac{R\cos(\varphi_P)}{2} \\ \frac{R}{W} & -\frac{R}{W} \end{bmatrix} \begin{bmatrix} \dot{q}_L \\ \dot{q}_R \end{bmatrix} \tag{13}$$

The equation (13) is given in the following form

$$\mathbf{A}(\mathbf{q_e})\dot{\mathrm{q}}_e = 0 \tag{14}$$

where $\mathbf{A}(\mathbf{q_e})$ vR^{3x6}

$$\mathbf{A}(\mathbf{q_e}) = \begin{bmatrix} \frac{R\sin(\varphi_P)}{2} & \frac{R\sin(\varphi_P)}{2} & -1 & 0 & 0 & 0 \\ -\frac{R\cos(\varphi_P)}{2} & -\frac{R\cos(\varphi_P)}{2} & 0 & -1 & 0 & 0 \\ \frac{R}{W} & -\frac{R}{W} & 0 & 0 & -1 & 0 \end{bmatrix} \tag{15}$$

The constraint formulation in (15) mathematically represents the nonholonomic constraints of the system. From a physical perspective, these constraints govern the vehicle's motion profile; in other words, they bound the admissible kinematic trajectories of the UGLV. Consequently, this kinematics-velocity coupling induces constraint forces, which will be thoroughly investigated within the framework of the dynamics section. Another noteworthy property is that these three kinematic constraints are linearly independent. Therefore, the constraint matrix $\mathbf{A}(\mathbf{q}_e)$ exhibits a full row rank of 3, a mathematical property that plays a critical role in subsequent multi-body dynamic formulations.

2.1.2. Inverse kinematics

Here, a simple inverse kinematics problem is chosen: let UGVLV move along a straight line segment AB while LV always aims at target M, as illustrated in Figure 3.

The yaw angle of the UGV and LV is determined as follows:

$$\varphi_P = \mathrm{atan}(\frac{y_B - y_A}{x_B - x_A});\ q_1 = \mathrm{acos}(\frac{\vec{AB}.\vec{PM}}{AB.PM}) \tag{16}$$

Choosing a trapezoidal speed control law with acceleration and deceleration times ts, the trajectory equation *s(t)* of the UGV is determined as follows:

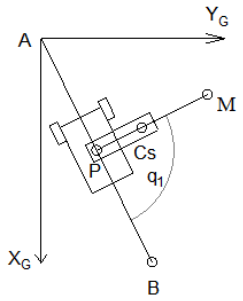


Figure 3. *Spatial configuration of the vehicle on the trajectory segment AB.*

$$s(t) = \begin{cases} s_0 + \frac{1}{2}a_m t^2 & 0 \le t \le t_s \\ s_0 - \frac{1}{2}a_m t_s^2 + a_m t_s t & t_s < t \le T - t_s \\ s_1 - \frac{1}{2}a_m T^2 + a_m T t - \frac{1}{2}a_m t^2 & T - t_s < t \le T \end{cases} \tag{17}$$

where s_0 signifies the initial position of the vehicle along the path; a_m is the constant magnitude of acceleration during both the startup and deceleration phases; and s_1 represents the total displacement, equivalent to the length of the segment AB.

2.2. Forward dynamics

The non-holonomic constraint is a form of force, and therefore it is added to the Lagrange equation.

$$\frac{d}{dt}\left(\frac{\partial T}{\partial \dot{\mathbf{q}}}\right)^T - \left(\frac{\partial T}{\partial \mathbf{q}}\right)^T = -\left(\frac{\partial \Pi}{\partial \mathbf{q}}\right)^T + \mathrm{Q} + \mathbf{A}^T(\mathbf{q_e})\boldsymbol{\lambda} \tag{18}$$

Consequently, the differential-algebraic equations of motion (18) can be compactly transformed into the standard matrix-vector formulation:

$$\mathbf{M}(\mathbf{q_e})\ddot{\mathbf{q}}_\mathbf{e} + \mathbf{C}(\mathbf{q_e},\dot{\mathbf{q}}_\mathbf{e})\dot{\mathbf{q}}_\mathbf{e} + \mathbf{G}(\mathbf{q_e}) = \mathbf{Q} + \mathbf{A}^T(\mathbf{q_e})\boldsymbol{\lambda} \tag{19}$$

where $\mathbf{M}(\mathbf{q_e})$ - The generalized inertia matrix; $\mathrm{C}\left(\mathrm{q}_e,\dot{\mathrm{q}}_\mathrm{e}\right)$: The Coriolis and centrifugal matrix; $\mathbf{G}(\mathbf{q_e})$ - The generalized potential force vector obtained from the gradient of the total potential energy; $\mathrm{Q}=\left[\tau_L \quad \tau_R \quad 0 \quad 0 \quad 0 \quad \tau_1\right]^T$ - The generalized active force vector [8].

To facilitate the numerical integration of the differential-algebraic equations of motion (19), it is necessary to eliminate the unknown Lagrange multipliers $\boldsymbol{\lambda}$, the constraint Jacobian matrix $\mathbf{A}(\mathbf{q_e})$ exhibits a full row rank of 3. Consequently, there exists an orthogonal matrix $\mathbf{S}(\mathbf{q_e})$ with a full column rank of 3 that spans the null-space of $\mathbf{A}(\mathbf{q_e})$, such that: $\mathbf{A}(\mathbf{q_e})\mathbf{S}(\mathbf{q_e}) = \mathbf{0}$

It is readily observed that:

$$\mathbf{S}(\mathbf{q_e}) = \begin{bmatrix} 1 & 0 & 0 \\ 0 & 1 & 0 \\ \dfrac{R\sin(\varphi_P)}{2} & \dfrac{R\sin(\varphi_P)}{2} & 0 \\ -\dfrac{R\cos(\varphi_P)}{2} & -\dfrac{R\cos(\varphi_P)}{2} & 0 \\ \dfrac{R}{W} & -\dfrac{R}{W} & 0 \\ 0 & 0 & 1 \end{bmatrix} \tag{20}$$

It can be seen that

$$\dot{\mathbf{q}}_\mathbf{e} = \mathbf{S}(\mathbf{q_e})\dot{\mathbf{q}}\,,\ \ddot{\mathbf{q}}_\mathbf{e} = \mathbf{S}(\mathbf{q_e})\ddot{\mathbf{q}} + \dot{\mathbf{S}}(\mathbf{q_e})\dot{\mathbf{q}} \tag{21}$$

Using Equation (21), multiplying both sides of Equation (19) by $\mathbf{S}^T$ yields

$$\mathbf{S}^T\mathbf{M}\mathbf{S}\ddot{\mathbf{q}} + \mathbf{S}^T(\mathbf{M}\dot{\mathbf{S}} + \mathbf{C}\mathbf{S})\dot{\mathbf{q}} + \mathbf{S}^T\mathbf{G} = \mathbf{S}^T\mathbf{Q} \tag{22}$$

Equation (22) can be written as

$$\mathbf{M}_n\ddot{\mathbf{q}} + \mathbf{C}_n\dot{\mathbf{q}} + \mathbf{G}_n = \mathbf{Q}_n \tag{23}$$

where the reduced dynamic matrices are defined as: $\mathbf{M}_n = \mathbf{S}^T\mathbf{M}\mathbf{S}$; $\mathbf{C}_n = \mathbf{S}^T(\mathbf{M}\dot{\mathbf{S}} + \mathbf{C}\mathbf{S})$; $\mathbf{G}_n = \mathbf{S}^T\mathbf{G}$; $\mathbf{Q}_n = \mathbf{S}^T\mathbf{Q} = \boldsymbol{\tau}$, với $\boldsymbol{\tau} = [\tau_L \quad \tau_R \quad \tau_1]^T$.

Combining equations (23) and (14) results in the complete differential-algebraic system of equations governing UGLV dynamics:

$$\begin{cases} \mathbf{M}_n\ddot{\mathbf{q}} + \mathbf{C}_n\dot{\mathbf{q}} + \mathbf{G}_n = \boldsymbol{\tau} \\ \mathbf{A}\dot{\mathbf{q}}_\mathbf{e} = 0 \end{cases} \tag{24}$$

and

$$\lambda = (\mathbf{A}\mathbf{M}^{-1}\mathbf{A}^T)^{-1}(\mathbf{A}\mathbf{M}^{-1}\left(\mathbf{C}\dot{\mathbf{q}}_\mathbf{e} + \mathbf{G} - \mathbf{Q}\right) - \dot{\mathbf{A}}\dot{\mathbf{q}}_\mathbf{e}) \tag{25}$$

Utilizing equation (25), the instantaneous magnitudes of the physical constraint forces $\boldsymbol{\lambda}$ can be explicitly computed at each time step, noting that $\boldsymbol{\lambda}$ depends strictly on the generalized positions and velocities of the redundant coordinate configuration $\mathbf{q_e}$.

2.3. Inverse dynamics

A core requirement for any practical autonomous system is to strictly satisfy its operational mission and functional requirements. For UGLV under consideration, the LV must continuously

maintain line-of-sight tracking toward a designated stationary target, while the UGV simultaneously navigates along a predefined spatial trajectory. The inverse dynamics problem investigates the system force behaviors and torque profiles necessary to satisfy these targeted functional specifications.

Within the framework of the inverse dynamics analysis, the reduced equations of motion (23) are formulated explicitly to calculate the input actuation torques as follows:

$$\boldsymbol{\tau} = \mathbf{M}_n\ddot{\mathbf{q}} + \mathbf{C}_n\dot{\mathbf{q}} + \mathbf{G}_n \tag{26}$$

3. RESULTS AND DISCUSSION

3.1. Forward kinematics and forward dynamics simulation

The UGLV parameter set is used for this simulation as follows:

W = 1 [m]; e = 0; H = 0,5 [m]; R = 0,2 [m]; h = 0,5 [m]; r = 0,2 [m]; m_L = 1 [kg]; $m_R = m_L$; m_P = 30 [kg]; m_S = 1 [kg]; g = 9,8 [m/s^2]; $I_{Lx} = 2.10^{-3}$ [kg.m^2]; $I_{Lz} = 3.10^{-3}$ [kg.m^2]; $I_{Rx} = I_{Lx}$; $I_{Rz} = I_{Lz}$; $I_{Px} = 4.10^{-2}$ [kg.m^2]; $I_{Py} = 3.10^{-2}$ [kg.m^2]; $I_{Pz} = 3.10^{-2}$ [kg.m^2]; $I_{Sz} = 0{,}5.10^{-3}$; $\tau_L = 0$; τ_R = -2 [N.m]; τ_1 = 0,5[N.m].

As illustrated in Figure 4, it is observed that the left and right wheels rotate in opposite directions when the driving torque is selectively applied only to the right wheel. Note that the rotational direction of the wheels is opposite to the forward translational motion of UGLV. Figure 5 indicates that the vehicle moves along a spiral trajectory, where the expansion rate of the spiral radius depends strictly on the applied driving torque.

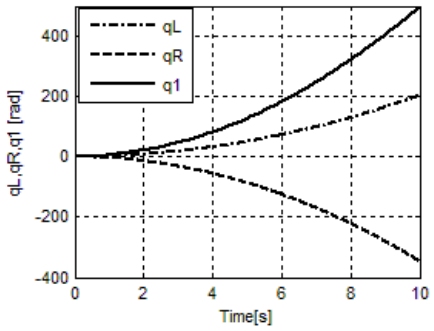


Figure 4. *Time histories of the left wheel, right wheel, and LV angular displacements.*

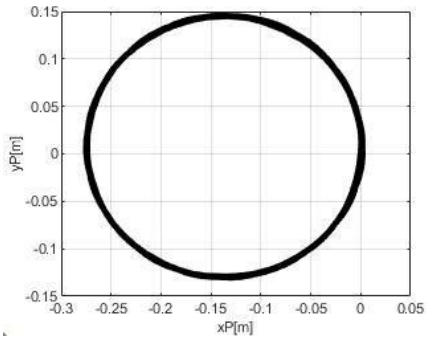


Figure 5. *Planar trajectory of UGLV under single-wheel actuation.*

The constraint forces λ_1 and λ_2 oscillate with an increasing amplitude over the time domain (Figure 6), whereas λ_3 remains invariant during the spiral trajectory of the robot. The progressive growth in the oscillation amplitude implies that as the radial displacement of the spiral path increases, the physical constraint forces required to maintain the non-slip wheel-ground contact aligned with the directional row vectors of the constraint Jacobian matrix $\mathbf{A}(\mathbf{q}_e)$ must scale up accordingly. Conversely, the joint constraint force keeps UGLV rotating stably about its own revolute axis remains stationary.

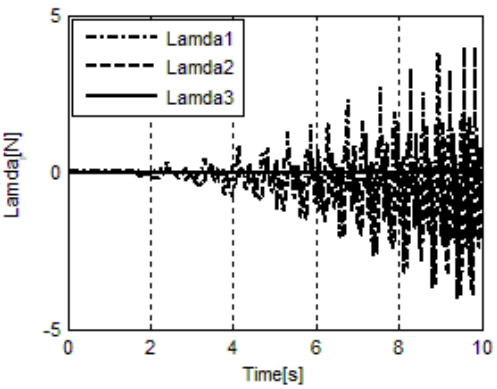


Figure 6. *Time histories of the Lagrange multipliers λ.*

3.2. Inverse kinematics and inverse dynamics simulation

During the simulation, the joint torques (τ_L, τ_R and τ_1) are determined based on a predefined motion trajectory and UGLV velocity profile. The UGLV configuration parameters are identical to those in the previous simulation, supplemented by the following parameters: $A(0;0)$; $B(4;2)$; $M(1;3)$; $t_s = 2$ [s]; $s_0 = 0$; $v_{max} = 0{,}5$ [m/s].

Based on these numerical inputs, the transient simulation results are obtained as follows:

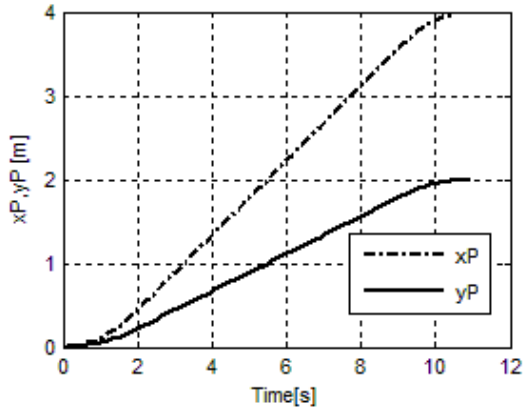


Figure 7. *Time histories of the global position coordinates x_P and y_P.*

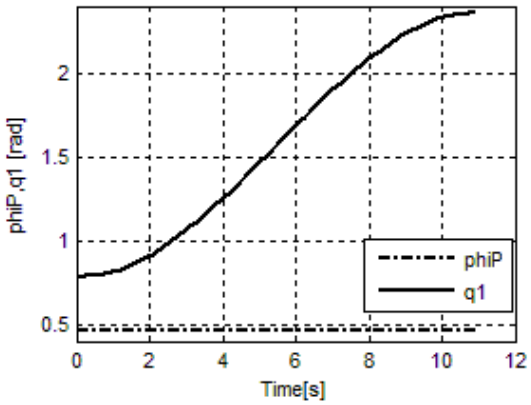


Figure 8. *Time histories of the orientation angles φ_P and q_1.*

The time histories of the generalized coordinates is illustrated Figures 7 and 8. x_P, y_P, and q_1 exhibit trends similar to $s(t)$, while φ_P remains constant as the UGLV moves along the straight line segment AB.

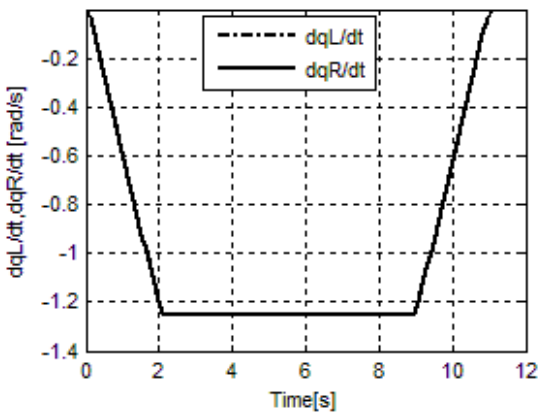


Figure 9. *Time histories of the left and right wheel angular velocities $\dot{q}_L$ and $\dot{q}_R$.*

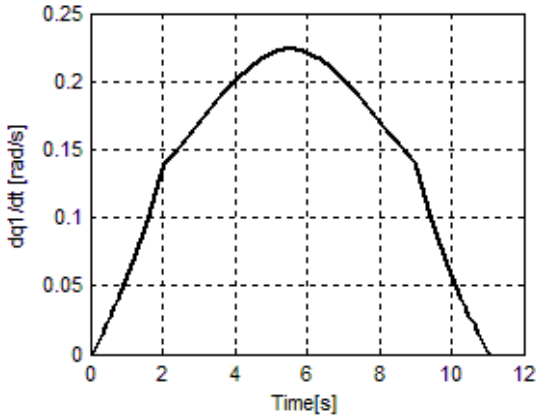


Figure 10. *Time history of the LV angular velocity* $\frac{dq_1}{dt}$.

The joint velocities of individual components initially increase and subsequently decrease over the time domain, as illustrated in Figures 9 and 10. This behavior agrees with the prescribed velocity of the UGV.

The joint torques over time are illustrated in Figures 11 and 12. This trend is consistent with the variation in the angular acceleration of the revolute joints. These profiles serve as a basis for selecting the corresponding motor parameters and mechanical design.

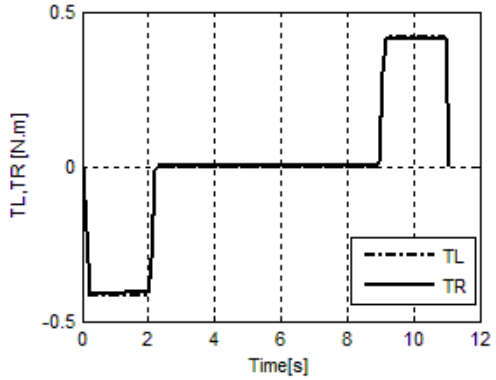


Figure 11. *Temporal evolution of the left and right wheel driving torques.*

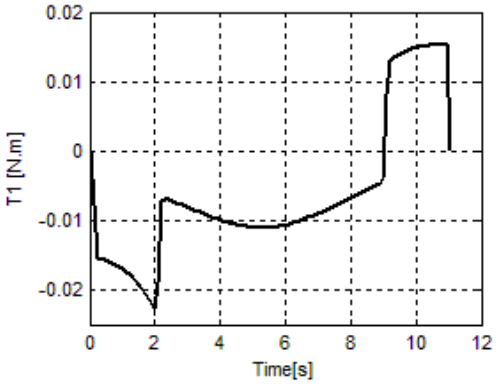


Figure 12. *Time history of the LV revolute joint driving torque.*

Furthermore, by evaluating the analytical closed-form expression (25), the corresponding verification results for the physical constraint forces $\boldsymbol{\lambda}$ are explicitly obtained and illustrated in the figures below.

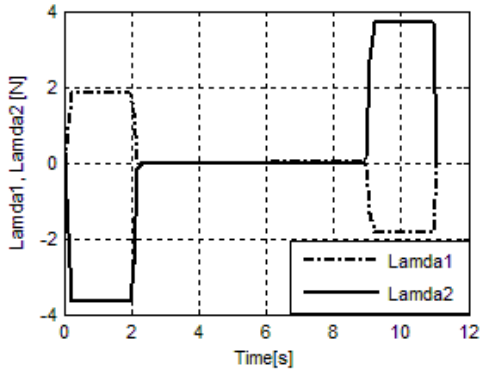


Figure 13. *Time histories of the Lagrange multipliers λ_1 and λ_2.*

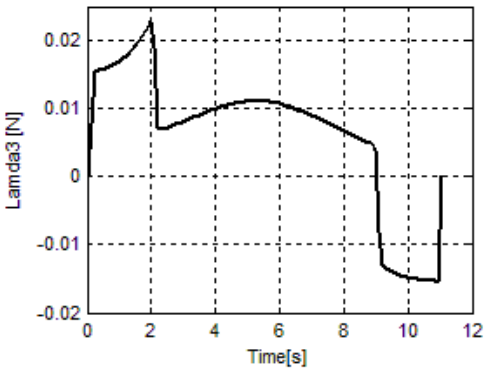


Figure 14. *Time history of the Lagrange multiplier λ_3.*

The constraint forces, as illustrated in Figure 13 and Figure 14, required to strictly satisfy the prescribed kinematic velocity profiles possess opposite signs (orientations) along the directional row vectors spanned by the constraint Jacobian matrix $\mathbf{A}(\mathbf{q}_e)$.

4. CONCLUSIONS

Based on the formulation of kinematic constraints and inverse kinematics ensuring that the LV mounted on UGV constantly tracks the target during motion and by applying the Lagrange equations with multipliers, the dynamic equations describing the motion of the UGLV have been successfully established in matrix form. Through mathematical transformations, redundant generalized coordinates were eliminated, and the multipliers were successfully decoupled and isolated, thereby clarifying the physical nature of these components. Application to a specific physical model initially demonstrates the validity of the developed mathematical model. These results serve as a foundation for structural design, as well as the design and synthesis of the control system for the UGLV.

Future research will focus on controller synthesis, simulation, analysis, and the development of the UGLV control system for real-world applications, building upon the verified dynamic model.

REFERENCES

[1]. Albagul and A. Wahyudi, *"Dynamic Modelling and Adaptive Traction Control for Mobile Robots"*, International Journal of Advanced Robotic Systems, 1, 3, pp. 169-178, (2004).

[2]. Chu Anh My et al, *"Mechanical Design and Dynamics Modelling of RoPC Robot"*, Proceedings of International Symposium on Robotics and Mechatronics, Ha Noi, Viet Nam, pp. 92-96, (2009).

[3]. Anna Jaskot and Bogdan, *"Dynamics of the mobile platform with four wheels drive"*, MATEC Web of Conferences, MATEC Web of Conferences 254, 03006, (2019).

[4]. Igor Zeidis and Klaus Zimmermann, *"Dynamics of a four-wheeled mobile robot with Mecanum wheels"*, ZAMM Journal of Applied Mathematics and Mechanics, (2019).

[5]. Jiri Balla, *"Dynamics of mounted automatic cannon on track vehicle"*, International Journal of Mathematical Models and Methods in Aplied Siences, 11, 3, (2011).

[6]. J. Dziopa, *"Modelling the Dynamics of a Mobile Land Robot"*, Problems of Mechatronics Armanent, Aviation, Safety Engineering, (2024).

[7]. Nguyễn Văn Khang, *"Động lực học hệ nhiều vật"*, Nhà xuất bản KHKT, Hà Nội, (2017) (in Vietnamese).

[8]. Trần Xuân Diệu và Nguyễn Xuân Thành, *"Nghiên cứu dao động của xe bệ phóng trên nền đàn hồi"*, TC. Nghiên cứu KHCNQS, 93, tr. 147-154, (2024) (in Vietnamese).

TÓM TẮT

Xây dựng mô hình động lực học phi hô-lô-nôm của thiết bị không người lái mặt đất mang thiết bị phóng

Trong bài báo này, mô hình động lực học phi holonomic của xe tự hành mặt đất (UGV) gắn bệ phóng (LV) được thiết lập dựa trên phương pháp phương trình Lagrange nhân tử. Mô hình động lực học ngược của hệ cơ học UGV-LV được xây dựng làm cơ sở để xác định các quy luật mô men trục bánh xe cần thiết cho việc bám quỹ đạo mục tiêu, cũng như bản chất động lực học của các nhân tử Lagrange. Mô hình động lực học tích hợp của hệ UGV-LV làm cơ sở cho việc thiết kế kết cấu của UGV-LV và tổng hợp bộ điều khiển.

Từ khoá: Thiết bị không người lái mặt đất; Phi hô-lô-nôm; Nhân tử Lagrange; Ma trận tựa đảo.